frontiers in Catalysis

ORIGINAL RESEARCH
published: 26 November 2021
doi: 10.3389/fctls.2021.781284

Biocatalytic Reductive Amination by Native Amine Dehydrogenases to Access Short Chiral Alkyl Amines and Amino Alcohols

*Laurine Ducrot[1], Megan Bennett[2], Adam A. Caparco[3], Julie A. Champion[3], Andreas S. Bommarius[3], Anne Zaparucha[1], Gideon Grogan[2] and Carine Vergne-Vaxelaire[1]**

[1]*Génomique Métabolique, Genoscope, Institut François Jacob, CEA, CNRS, Univ Evry, Université Paris-Saclay, Evry, France,* [2]*York Structural Biology Laboratory, Department of Chemistry, University of York, York, United Kingdom,* [3]*School of Chemical and Biomolecular Engineering, Georgia Institute of Technology, Atlanta, GA, United States*

Small optically active molecules, and more particularly short-chain chiral amines, are key compounds in the chemical industry and precursors of various pharmaceuticals. Their chemo-biocatalytic production on a commercial scale is already established, mainly through lipase-catalyzed resolutions leading to ChiPros™ products among others. Nevertheless, their biocatalytic synthesis remains challenging for very short-chain C4 to C5 amines due to low enantiomeric excess. To complement the possibilities recently offered by transaminases, this work describes alternative biocatalytic access using amine dehydrogenases (AmDHs). Without any protein engineering, some of the already described wild-type AmDHs (*Cfus*AmDH, *Msme*AmDH, *Micro*AmDH, and MATOUAmDH2) were shown to be efficient for the synthesis of hydroxylated or unfunctionalized small 2-aminoalkanes. Conversions up to 97.1% were reached at 50 mM, and moderate to high enantioselectivities were obtained, especially for (*S*)-1-methoxypropan-2-amine (98.1%), (*S*)-3-aminobutan-1-ol (99.5%), (3*S*)-3-aminobutan-2-ol (99.4%), and the small (*S*)-butan-2-amine (93.6%) with *Msme*AmDH. Semi-preparative scale-up experiments were successfully performed at 150 mM substrate concentrations for the synthesis of (*S*)-butan-2-amine and (*S*)-1-methoxypropan-2-amine, the latter known as "(*S*)-MOIPA". Modeling studies provided some preliminary results explaining the basis for the challenging discrimination between similarly sized substituents in the active sites of these enzymes.

Keywords: native amine dehydrogenases, reductive amination, short chiral amines, amino alcohols, (*S*)-MOIPA, (S)-butan-2-amine

OPEN ACCESS

Edited by:
Francesca Paradisi,
University of Bern, Switzerland

Reviewed by:
Elaine O'Reilly,
University College Dublin, Ireland
Jan von Langermann,
University of Rostock, Germany

****Correspondence:***
Carine Vergne-Vaxelaire
carine.vergne@genoscope.cns.fr

Specialty section:
This article was submitted to Biocatalysis, a section of the journal Frontiers in Catalysis

Received: *22 September 2021*
Accepted: *29 October 2021*
Published: *26 November 2021*

Citation:
Ducrot L, Bennett M, Caparco AA, Champion JA, Bommarius AS, Zaparucha A, Grogan G and Vergne-Vaxelaire C (2021) Biocatalytic Reductive Amination by Native Amine Dehydrogenases to Access Short Chiral Alkyl Amines and Amino Alcohols. Front. Catal. 1:781284. doi: 10.3389/fctls.2021.781284

INTRODUCTION

Short-chain chiral amines with carbon chain lengths ranging from C1 to C5 have a wide range of applications in the chemical industry as precursors of pharmaceuticals and agrochemicals (Wu et al., 2021). For example, the butan-2-amine substructure is present in the herbicide Bromacil commercialized as the racemate and in the drug candidate XL888. When substituted with a hydroxyl group, the resulting highly functionalized chiral amino alcohols serve as chiral auxiliaries or ligands in various asymmetric syntheses (Ager et al., 1996). Key examples of these

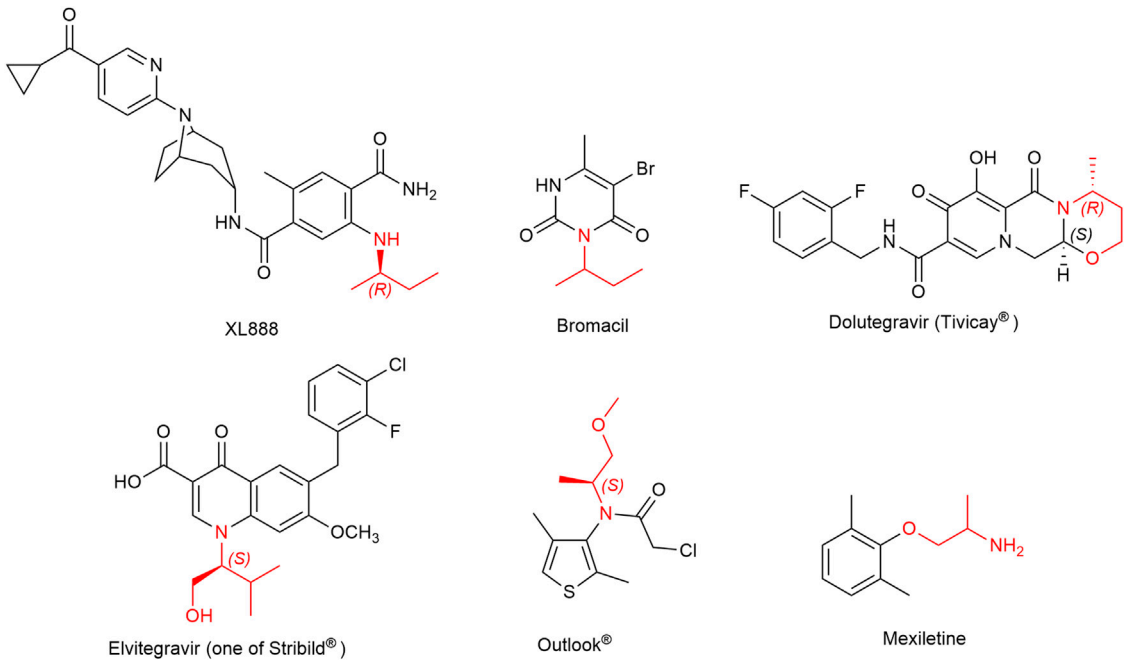

FIGURE 1 | Structures of some active components of pharmaceuticals and agrochemicals containing short chiral amines. The chiral amino moieties are highlighted in red.

important structural moieties are L-valinol and (*R*)-3-aminobutan-1-ol ((*R*)-ABOL), intermediates in the synthesis of HIV integrase inhibitors Elvitegravir (Japan Tobacco, Gilead Sciences) and Dolutegravir (GSK, Pfizer, Shionogi Limited) respectively, (*S*)-MOIPA, a key chiral element within the herbicide Outlook® (BASF), or 2-aminopropan-1-ol, the main building block of the antiarrhythmic agent Mexiletine (**Figure 1**).

All of these key small chemical entities are industrially produced by well-established traditional synthetic routes, but green alternatives such as biocatalytic access are topics of great interest in the current context of waste reduction and sustainable chemistry. The ChiPros™ process of BASF based on lipase-catalyzed acetylation is highly efficient for the kinetic resolution of many alkyl amines, such as (*S*)-1-phenylbutylamine or (*S*)-2-aminononane, with *E* values of >1,000. Nevertheless, in the case of small alkyl amines, *E* values are much lower ($E_{\text{butan-2-amine}}$ = 8, $E_{(R)\text{-ABOL}}$ << 10, $E_{2\text{-aminopentane}}$ = 50, and $E_{3\text{-methylbutan-2-amine}}$ = 80) due to the similar size of the R-groups, and their resolution requires more expensive acyl donors or solvents. Therefore, biocatalyzed enantioselective syntheses of these molecules are particularly challenging. Some success has already been reported with transaminases (TAs). BASF has completed the process development of (*R*)-ABOL 2.0 with *ee* values of >99.9% (Ditrich, 2020). Kroutil and colleagues have produced both enantiomers of Mexiletine in up to >99% *ee* by deracemization using ω-TA transaminase chemistry (Koszelewski et al., 2009), and (*R*)- or (*S*)-butan-2-amine has been efficiently synthesized by continuous-flow chemistry using covalently immobilized transaminases *RTA-43 and HEwT_F84W, respectively (Heckmann et al., 2021). ω-Transaminases have also been proved to be useful tools for the asymmetric amination of α-hydroxy ketones, either alone or in cascade reactions for the synthesis of chiral vicinal amino alcohols (Gomm and O'Reilly, 2017; Slabu et al., 2017; Patil et al., 2018a). The requirement of transaminases for the addition of an excess of the amino donor that is sacrificed during the process alongside *in situ* by-product removal or *in situ* product removal for example using supported liquid membrane (Rehn et al., 2016) pushed the search for alternative enzymes. Enzymes performing proper reductive amination have emerged as promising biocatalysts for the synthesis of optically active amines. Thanks to the recent discovery of native Amine Dehydrogenases (AmDHs) and Reductive Aminases (RedAms), such enzymes are no longer restricted to engineered Amino Acid Dehydrogenases (engAADHs) (Ye et al., 2015; Patil et al., 2018b; Cheng et al., 2020; Ducrot et al., 2020; Cosgrove et al., 2021; Mutti and Knaus, 2021). Although they are described to be active toward a wide range of carbonyl-containing compounds, only a few examples are reported for the synthesis of small chiral alkyl amines and small amino alcohols. These include the engineered L-AmDH-TV (mutant D32A/F101S/C290V of L-AmDH) (Franklin et al., 2020) and the mutant AmDH-M_0 (mutant K68T/N261L of *Lf*LeuAADH) (Chen et al., 2019). We recently described native AmDHs from biodiversity and provided a picture of their substrate scope (Mayol et al., 2019; Caparco et al., 2020). Their top tested substrates were mainly cyclohexanone and isobutyraldehyde, but some of them displayed activity toward alkyl linear ketones such as pentan-2-one enabling the biocatalytic synthesis of the corresponding (*S*)-amines on a

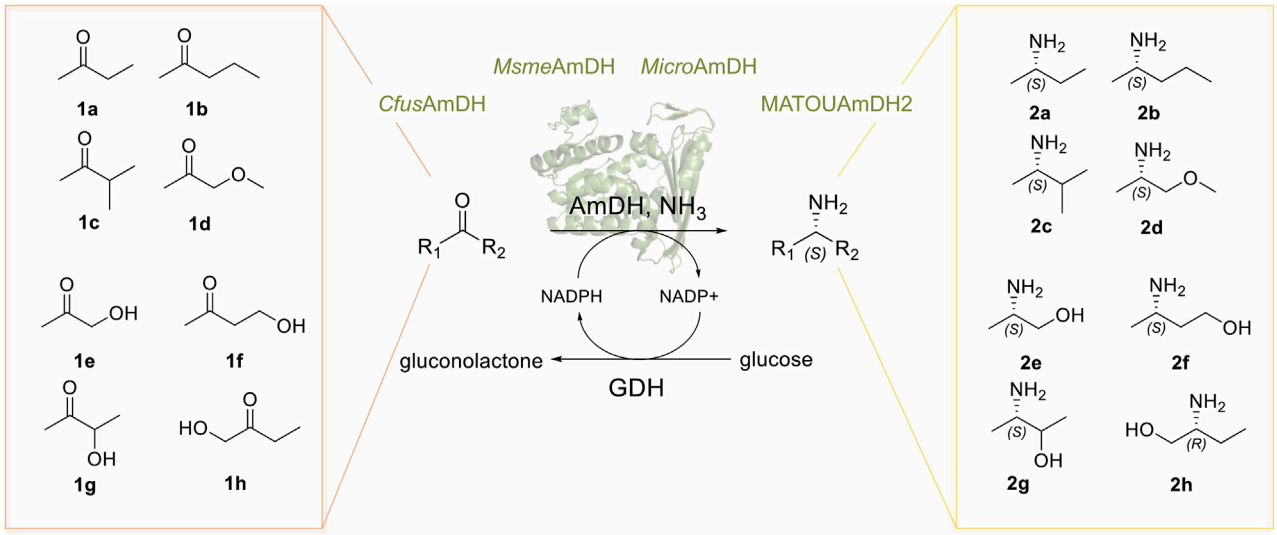

FIGURE 2 | Reductive amination reactions catalyzed by native AmDHs detailed in this study. GDH = glucose dehydrogenase.

millimolar scale (Mayol et al., 2019). The high enantiomeric excess (*ee* > 97%) in favor of the (*S*)-amines obtained in these cases prompted us to consider that high enantioselectivity could be achieved for other small chiral amines. In the present work, we sought to study in more detail the biocatalytic potential of some of these native AmDHs (*Cfus*AmDH, *Msme*AmDH, *Micro*AmDH, and MATOUAmDH2) for the synthesis of small chiral alkyl amines and small amino alcohols **2a–h** (**Figure 2**).

MATERIALS AND METHODS

Chemicals and Materials

All reagents were purchased from commercial sources and used without additional purification, except in-house (*S*)-pentan-2-amine (*S*)-**2b** (Mayol et al., 2019). Butan-2-one (**1a**), pentan-2-one (**1b**), 1-methoxypropan-2-one (**1d**), 4-hydroxybutan-2-one (**1f**), 1-hydroxypropan-2-one (**1e**), 3-hydroxybutan-2-one (acetoin; **1g**), 2-aminopropan-1-ol (alaninol; **2e**), butan-2-amine (**2a**), pentan-2-amine (**2b**), 3-methylbutan-2-amine (**2c**), 1-methoxypropan-2-amine (**2d**), 2-aminobutan-1-ol (**2h**), (*S*)-butan-2-amine ((*S*)-**2a**), (*R*)-3-methylbutan-2-amine ((*R*)-**2c**), (*S*)-1-methoxypropan-2-amine ((*S*)-**2d**), (*S*)-2-aminopropan-1-ol (*S*-alaninol; (*S*)-**2e**), (*S*)-2-aminobutan-1-ol ((*S*)-**2h**), β-nicotinamide adenine dinucleotide phosphate disodium salt ($NADP^+$), glucose dehydrogenase (GDH105), (*S*)-2-(5-fluoro-2,4-dinitrophenylamino)propanamide (FDAA), and benzoyl chloride (BzCl) were purchased from Merck/Sigma-Aldrich (St. Louis, MO, United States). 3-Methylbutan-2-one (**1c**), 1-hydroxybutan-2-one (**1h**), 3-aminobutan-1-ol (**2f**), 3-aminobutan-2-ol (**2g**), (*R*)-3-aminobutan-1-ol ((*R*)-**2f**), and (2*R*,3*S*)-3-aminobutan-2-ol ((2*R*,3*S*)-**2g**) were purchased from Enamine Ltd. (Kiev, Ukraine). Buffers were produced from substances purchased from Sigma–Aldrich and adjusted to the desired pH value with ammonium hydroxide 30%. UHPLC-UV analysis were performed on a UHPLC U3000 RS 1034 bar system (Thermo Fisher Scientific, Waltham, MA, United States) equipped with a UV detector, using a Kinetex F5 column (100 mm × 2.1 mm; 1.7 µm) (Phenomenex, California, United States). NMR spectra were recorded on a Bruker (Bruker, Billerica, MA, United States) 600-MHz spectrometer (Evry University, France) for ^1H and ^{13}C experiments. Chemical shifts (expressed in ppm) of ^1H and ^{13}C spectra were referenced to the solvent peak δ (H) = 4.79 for D_2O.

Large-Scale Purification of Amine Dehydrogenases

Large-scale purification of *Msme*AmDH, *Cfus*AmDH, *Micro*AmDH, and MATOUAmDH2 was conducted using 2 × 500 ml culture by nickel affinity chromatography (His Trap FF 5 ml) in tandem with gel filtration (Hi Load 16/60 Superdex 200pg) as described elsewhere (Mayol et al., 2019). The storage buffer was 50 mM NaCl, 50 mM sodium phosphate pH 7.5–8.0, glycerol 10%–15%, and 1 mM DTT. Protein concentrations were determined by the Bradford method with bovine serum albumin as the standard (Bradford, 1976). The samples were analyzed by SDS-PAGE using the Invitrogen NuPAGE system. The purified proteins were stored at −80°C.

Screening of *Msme*AmDH, *Cfus*AmDH, *Micro*AmDH and MATOUAmDH2 for Conversion of Short Alkyl (Hydroxyl) Ketones

The selected AmDHs (*Cfus*AmDH, *Msme*AmDH, *Micro*AmDH, and MATOUAmDH2), were tested toward ketones **1a**–**1h** in a 96-well plate with a cofactor regeneration system using UHPLC-UV monitoring. To a reaction mixture (total volume = 100 µl) containing 0.2 mM $NADP^+$, 11 mM or 55 mM glucose (1.1 eq.),

and 3 U ml^{-1} GDH105 in 2 M NH_4HCO_2 buffer, pH 9.0, was added 10 mM or 50 mM (final concentration) of substrate followed by 0.5 mg ml^{-1} of purified AmDH. The 96-well plate was covered with an aluminum thermowell sealer and a lid and left for 24 h at 30°C in a thermocontrolled oven. The 96-well plate contained wells with background reactions performed in the same manner but lacking the substrate or the purified AmDH, together with wells with calibration mixtures containing 2 M NH_4HCO_2 buffer pH 9.0 and various concentrations of amines (2, 4, 6, and 8 mM for 10 mM reactions and 10, 20, 30, and 40 mM for 50 mM reactions). All the wells were analyzed by UHPLC-UV after derivatization with BzCl in 96-well plates. The amounts of amines in reaction mixtures were deduced from calibration curves obtained from the UV-response of the calibration mixtures of racemic **2a**–**2h** (**Supplementary Figures S1, S2**). Enantiomeric excess of products **2a**–**2h** and diastereoisomeric excess for **2g** were determined after derivatization with FDAA in 96-well plates for UHPLC-UV detection (**Supplementary Figure S3**). The reactions were performed in duplicate or triplicate at different days to ensure reliable reproducibility.

Derivatization Procedures and UHPLC-UV Conditions

BzCl derivatization: 20 µl of each reaction mixture was mixed with 50 µl of a 200 mM Na_2CO_3/$NaHCO_3$ aqueous solution, pH 9.5, and then mixed with 30 µl of a 50 mM BzCl solution in acetonitrile (MeCN). The derivatization reaction was left for 40 min at room temperature for reactions in a 96-well plate (or vortexed for 30 s in case of reactions in microtubes) and then quenched by the addition of 20 µl of a 1 M HCl aqueous solution and 30 µl of a 1/1 solution of H_2O/ACN. After centrifugation (1,008 *g*, 5 min, 4°C) on a 0.22-µm filtration 96-well plate (or with 0.22-µm syringe filters in case of derivatization in microtubes), the filtrates were analyzed by UHPLC-UV (eluent MeCN/H_2O + 0.1% formic acid with a linear gradient 20/80 during 1 min, then 20/80 to 70/30 in 3 min, then 70/30 during 2 min followed by re-equilibration time; flow 0.5 ml min^{-1}; temperature 25°C; injection volume 3 µl; λ = 250 nm).

FDAA derivatization: 20 µl of each reaction mixture was mixed with 8 µl of a 1 M $NaHCO_3$ aqueous solution, pH 8.0, and then mixed with 20 µl of a 15 mM FDAA solution in 1/1 acetone/EtOH. The derivatization reactions were left 2 h at 55°C for reactions in a 96-well plate (or stirred at 600 rpm for 2 h at 65°C in case of reactions in microtubes), and then quenched by the addition of 4 µl of a 2 M HCl aqueous solution and 80 µl of a 1/1 solution of H_2O/MeOH. After centrifugation (1,008 *g*, 5 min, 5°C) on a 0.22-µm filtration 96-well plate (or with 0.22 µm syringe filters in case of derivatization in microtubes), the filtrate was analyzed by UHPLC-UV (eluent MeOH/H_2O + 0.1% formic acid with a linear gradient 40/60 to 80/20 in 5 min, then 80/20 during 3 min followed by re-equilibration time; flow 0.3 ml min^{-1}; temperature 25°C; injection volume 3 µl; λ = 340 nm). In the case of **2a**, the eluent was as follows: a linear gradient 30/70 to 80/20 in 10 min, then 80/20 during 3 min followed by re-equilibration time.

Effect of Substrate Loadings on Conversion of 1-Methoxypropan-2-one and Butan-2-one

The tolerance of *Msme*AmDH to higher substrate concentrations was studied by monitoring the conversion of 1-methoxypropan-2-one (**1d**) into (*S*)-1-methoxypropan-2-amine (**2d**) and butan-2-one (**1a**) to (*S*)-butan-2-amine (**2a**) for 24–48 h. Reaction mixtures (100 µl), containing 0.2 mM $NADP^+$, 1.1 eq. of glucose, 3 U ml^{-1} GDH105 in 2 M NH_4HCO_2 buffer, pH 9.0, 0.5 mg ml^{-1} or 1 mg ml^{-1} of purified *Msme*AmDH, and substrate at a concentration range of 50 to 200–300 mM, were incubated in microtubes at 30°C at 400 rpm. Aliquots were taken at 24 and 48 h and diluted in 2 M NH_4HCO_2 buffer, pH 9.0, to reach theoretically 50 mM (or 10 mM for *ee* value determination) product concentration. Conversion to (*S*)-amines and *ee* values was determined in 96-well plates by UHPLC-UV after derivatization with BzCl and FDAA, respectively.

Semi-Preparative Scale Reactions

1d to **2d**: In a 50-ml Greiner tube equipped with a screw cap was poured 1-methoxypropan-2-one (**1d**) (7.50 ml of a 1 M stock solution in water, 1 eq., 7.5 mmol), distilled water (14.90 ml), NH_4HCO_2 buffer, pH 9.0 (10.00 ml of a 10 M stock solution), $NADP^+$ (2.00 ml of a 5 mM stock solution, 0.001 eq., 0.01 mmol), glucose (9.27 ml of a 0.89 M stock solution, 1.1 eq., 8.25 mmol), GDH105 (1.5 ml of a 100 U ml^{-1} stock solution), and *Msme*AmDH purified by gel filtration (4.83 ml of a 5.2 mg ml^{-1} stock solution). The reaction was shaken at 30°C, 300 rpm with UHPLC-UV monitoring after BzCl derivatization in microtubes (**Supplementary Figures S4, S5**). Isolation of the product **2d** was not performed.

1a to **2a**: In a 50-ml Greiner tube equipped with a screw cap was poured butan-2-one (7.50 ml of a 1 M stock solution in water, 1 eq., 7.5 mmol), distilled water (15.92 ml), NH_4HCO_2 buffer, pH 9.0 (10.00 ml of a 10 M stock solution), $NADP^+$ (2.00 ml of a 5 mM stock solution, 0,001 eq., 0.01 mmol), glucose (8.25 ml of a 1 M stock solution, 1.1 eq., 8.25 mmol), GDH105 (1.5 ml of a 100 U ml^{-1} stock solution), and *Msme*AmDH purified by gel filtration (4.83 ml of a 5.2 mg ml^{-1} stock solution). The reaction was shaken at 30°C, 300 rpm with UHPLC-UV monitoring after BzCl derivatization in microtubes. After 24 h, the reaction was acidified to pH 1–2 with concentrated HCl and concentrated *in vacuo* to remove unreacted ketone (water bath 45°C, p = 35 mbar). After addition of 10 ml of water, the mixture was basified with KOH 10 M under cooling by ice bath and distilled under atmospheric pressure. Three fractions were collected [fraction 1: boiling point (bp) 65–70°C, fraction 2: bp 70–80°C, fraction 3: bp 80–85°C]. The three fractions were analyzed by UHPLC-UV and NMR demonstrating the presence of the desired product with more or less water and ammonia salt. The three fractions were combined, acidified with concentrated HCl (approximatively 2 eq.), and lyophilized. The (2*S*)-butan-2-amine (**2a**) was obtained as monohydrochloride salt (421 mg, 51% yield, white solids) with 92.6% *ee* as determined by UHPLC-UV after FDAA derivatization (**Supplementary Figures S6–S8**). NMR

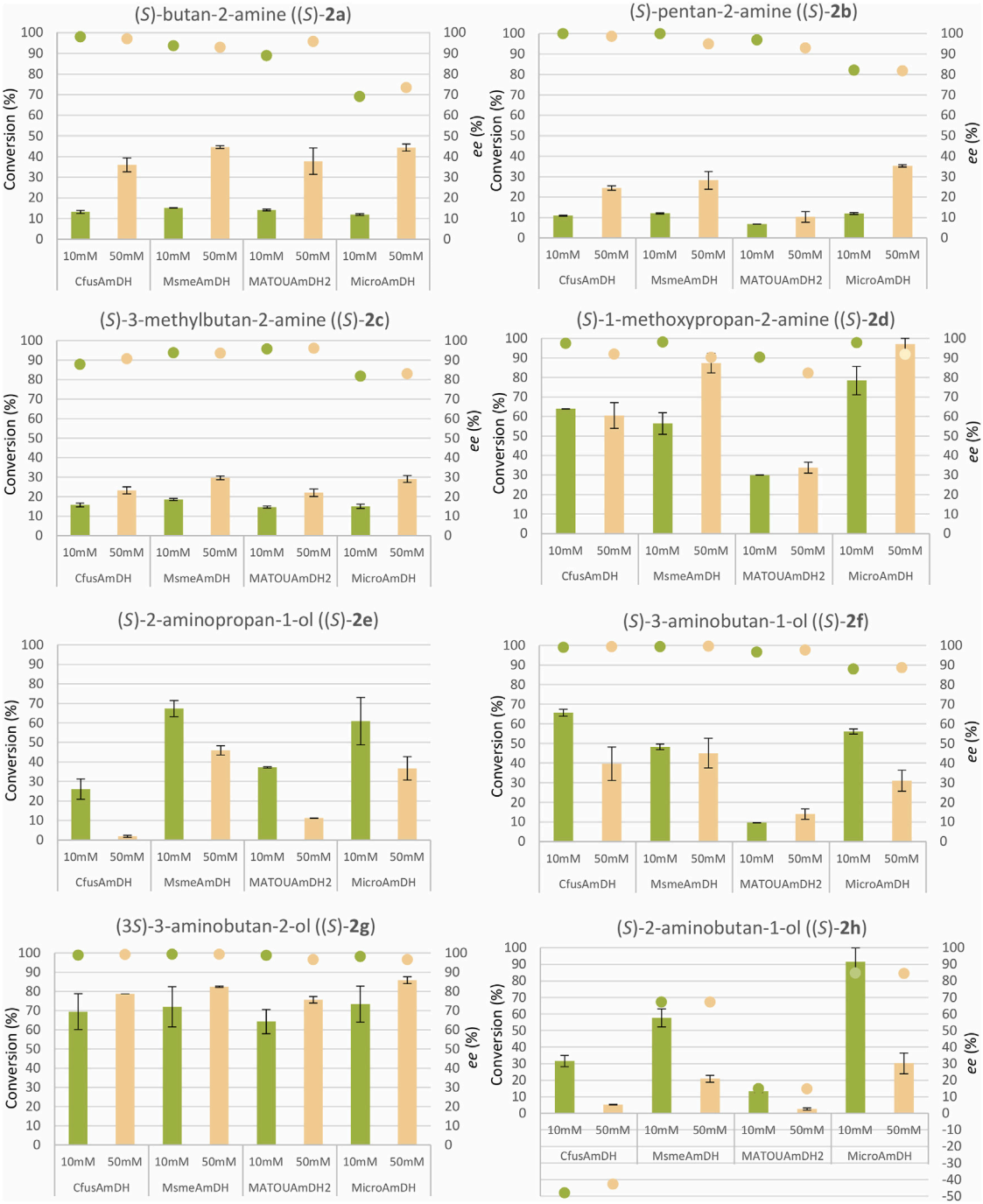

FIGURE 3 | Conversions and enantiomeric excess results with *Cfus*AmDH, *Msme*AmDH, MATOUAmDH2, and *Micro*AmDH. Reactions conditions: 10 mM or 50 mM substrate, 2 M NH_4HCO_2 buffer, pH 9.0, 0.2 mM $NADP^+$, 1.1 eq. glucose, 3 U ml^{-1} GDH105, 0.5 mg ml^{-1} purified AmDH, 24 h, 30°C. Error bars represent standard deviations of two or three independent experiments. Due to coelution with FDAA-derivatized co-product, the enantiomeric excess of (*S*)-2-aminopropan-1-ol (**2e**) could not be calculated, but the (*S*)-enantiomer was the major peak (**Supplementary Figure 3E**). The data are given in **Supplementary Figure S13**.

spectra were identical to standard amine commercially available. ^{1}H NMR (600 MHz, D_2O) δ 3.31 (m, 1H), 1.57–1.73 (m, 2H), 1.29 (d, *J* = 6.74 Hz, 3H), 0.98 (t, *J* = 7.60 Hz, 3H). ^{13}C NMR (150 MHz, D_2O) δ 49.3, 27.2, 17.2, 9.0. (**Supplementary Figures S9–S12**).

Modeling and Docking Experiments

The products (*R/S*)-butan-2-amine (**2a**), (*2R/S*)-2-amino-1-propanol (**2e**), and (*2R/S*)-2-aminobutanol (**2h**) were docked into the structures *Msme*AmDH and *Cfus*AmDH, and into the models of *Micro*AmDH and MATOUAmDH2 to analyze the

observed stereoselectivities. Each amine product was docked as their (*R*)- and (*S*)-enantiomers separately. The ligand PDB files were generated using the CORINA Molecular Online Tool. The docking was done in the RX structures of *Cfus*AmDH (PDB: 6IAU) and *Msme*AmDH (PDB: 6IAQ) and in the homology models generated for *Micro*AmDH (PDB template used: 6IAQ) and MATOUAmDH2 (PDB template used: 6IAU) using SWISS-MODEL. With AutoDockTool (Morris et al., 2009), the docking simulations were performed on rigid structures, with no flexibility given to any catalytic pocket residues. The number of Genetic Algorithm (GA) runs were fixed at 50 using the Lamarckian GA (4.2). The 50 ligand conformations obtained were then analyzed in PyMOL.

RESULTS

Conversions of Various Small Alkyl and Hydroxylated Ketones

In the context of biocatalytic applications, we aim to explore the synthetic potential of native AmDHs already described mainly through determination of specific activities and kinetic parameters. The AmDHs *Msme*AmDH, *Cfus*AmDH, *Micro*AmDH, and MATOUAmDH2, selected according to their reported substrate profiles, were tested with a cofactor recycling system over 24 h to provide conversion data with the small alkyl ketones, butan-2-one (**1a**), pentan-2-one (**1b**), 3-methylbutan-2-one (**1c**), 1-methoxypropan-2-one (**1d**), 1-hydoxypropan-2-one (**1e**), 4-hydroxybutan-2-one (**1f**), 3-hydroxybutan-2-one (**1g**), and 1-hydroxybutan-2-one (**1h**). Each substrate was tested at 10 and 50 mM to provide preliminary data for biocatalytic syntheses at a more substantial substrate concentration, while using a reasonable amount of purified enzyme (0.5 mg ml^{-1}). All reactions were carried out in 96-well plates at 30°C in ammonium formate buffer, pH 9.0, with a glucose–glucose dehydrogenase $NADP^+$ recycling system. The conversions were calculated based on calibration curves obtained with commercialized standards after derivatization of the reaction mixtures with BzCl and UHPLC-UV analysis performed in 96-well plates. The enantiomeric excesses were calculated after UHPLC-UV analysis of the same reactions derivatized with FDAA in a 96-well plate.

The results are shown in **Figure 3** and detailed in **Supplementary Figure S13**. At 10 mM, low conversions (6.8%–18.5%) were obtained for small alkyl ketones devoid of any functionality, but interestingly, high *ee* values (96.0 and 98.1% respectively) were still recorded in the case of the smallest amine (*S*)-butan-2-amine (**2a**) with *Msme*AmDH and *Cfus*AmDH, despite the high similarity between the size of each substituent. We note that MATOUAmDH2 and especially *Micro*AmDH gave lower *ee* values (88.9% and 69.1%, respectively). Conversions and enantioselectivity results for (*S*)-pentan-2-amine (**2b**) were similar to that previously described for *Cfus*AmDH, despite lower conversions observed experimentally in plates compared to closed microtubes, presumably due to undesired evaporation of the substrate. Very interestingly, good to high conversions of 1-methoxypropan-2-one (**1d**) to the corresponding amine (*S*)-MOIPA (**2d**) were achieved with *Cfus*AmDH (63.9%), *Msme*AmDH (56.5%), and *Micro*AmDH (78.4%). Lower conversions were obtained with MATOUAmDH2 (30.0%), together with slightly lower *ee* values (90.4% against 97.4–98.1) for the three other enzymes. Even more remarkable were the moderate to high conversions obtained with non-protected alcohols. With 10 mM as the starting substrate concentration, the small vicinal amino alcohol (3*S*)-3-aminobutan-2-ol (**2g**) was obtained with 64.3%–73.3% conversion with the four tested enzymes. For ketones **1e**, **1f**, and **1h** with a terminal alcohol, the conversions were much more dependent on the enzyme. (*S*)-2-aminopropan-1-ol (**2e**) and (*S*)-2-aminobutan-1-ol (**2h**) were formed with low to moderate conversions with *Cfus*AmDH and MATOUAmDH2 (26.1%–31.6% and 37.2%–13.4%, respectively) whereas good conversions were reached with *Msme*AmDH and *Micro*AmDH (67.4%–57.6% and 60.9%–91.5%, respectively). (*S*)-3-aminobutan-1-ol (**2f**) was formed with only 9.6% with MATOUAmDH2, but with 48.2%–65.7% with the other three AmDHs. High stereoselectivity in favor of the (*S*)-enantiomer were confirmed for all these substrates with *ee* values generally above 96%, except for 2-aminobutan-1-ol (**2h**) for which an (*R*)- preference was determined in the case of *Cfus*AmDH, even if the enantiomeric excess was quite low (48.1%). Taking into account Cahn-Ingold-Prelog rules, this is in accordance with the same positioning of the longest carbon chain of the substrate in the active site. For *Msme*AmDH and *Micro*AmDH, the (*S*)-amines were formed with 67.0%–84.8% *ee*, whereas only 14.9% *ee* was measured with MATOUAmDH2, in addition to low conversion. Excellent *ee* values (98.8%–99.4%) were particularly obtained for (3*S*)-3-aminobutan-2-ol (**2g**) with *Cfus*AmDH, *Msme*AmDH and MATOUAmDH2 (98.2% with *Micro*AmDH). In case of this chiral substrate, bad diasteroisomeric excess was obtained with the four enzymes (10.4%–13.0%, **Supplementary Figure S13**) showing that they accept both enantiomers at the alcohol position. Overall, *Micro*AmDH displayed lower enantioselectivities compared to the three other enzymes, particularly for alkylketones **2a**–**2c** and for 2-aminopropan-1-ol (**2e**). For the former, the not quantified (*R*)-enantiomer was present in larger amounts with *Micro*AmDH than with other enzymes, for which only traces could be detected. We noted that the four enzymes did not differentiate the stereochemistry at the vicinal OH position, with the *trans*/*cis* ratio ranging from 55.2% to 56.5%.

At 50 mM substrate, all the conversions were similar or even much higher compared with 10 mM for substrates **1a**–**1d** without any free hydroxyl group, at equivalent concentration of biocatalyst. The conversion of butan-2-one (**1a**) was 2.7–3.7 times higher at 50 mM than at 10 mM. For the one and two more carbon substrates **1b** and **1c**, this behavior was also observed but to a lesser extent (1.5–3 times for **1b** and 1.5–1.9 times for **1c**). With free hydroxylated ketones **1e**–**1h**, the increase in substrate concentration was tolerated by the four enzymes for 4-hydroxybutan-2-one (**1f**) and 3-hydroxybutan-2-one (**1g**) but not for 1-hydoxypropan-2-one (**1e**) and 1-hydroxybutan-2-one (**1h**), where significant decreases in conversion were observed. Among the four tested enzymes, *Cfus*AmDH seemed to be the most affected. In terms of enantiomeric excess, overall, the ratio between enzymes for all the tested substrates was approximately conserved.

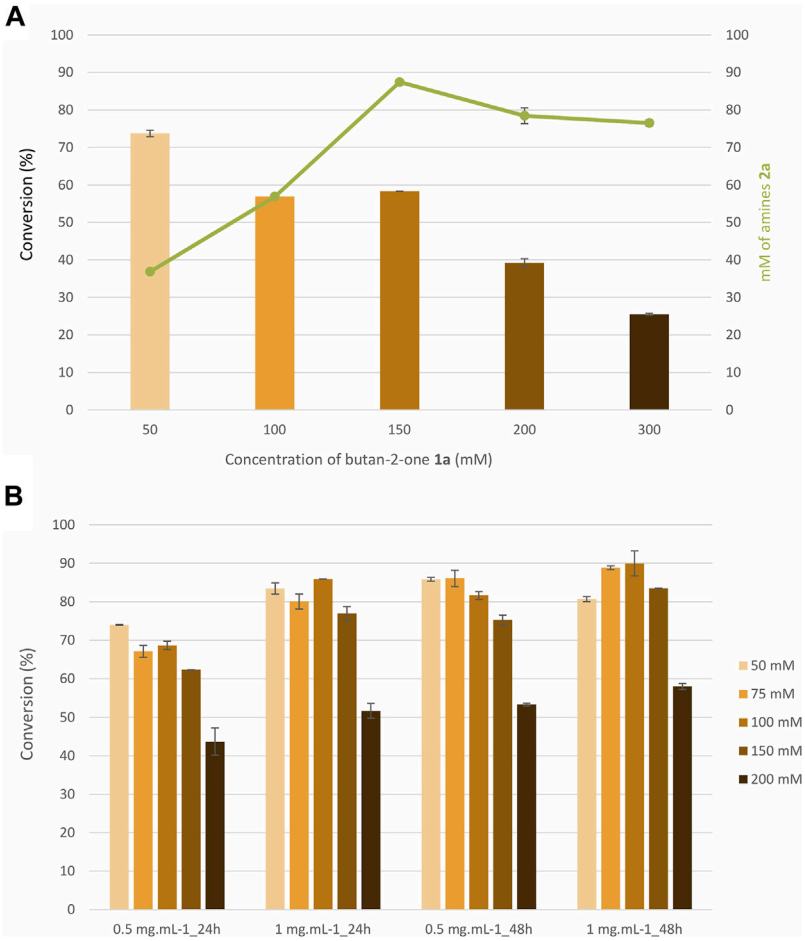

FIGURE 4 | (A) and **(B)** Effect of concentration in butan-2-one 1a **(A)** and 1-methoxypropan-2-one 1d **(B)** on the conversion with *Msme*AmDH. Reactions conditions: 10–200 mM substrate, 2 M NH_4HCO_2 buffer, pH 9.0, 0.2 mM $NADP^+$, 1.1 eq. glucose, 3 U ml^{-1} GDH105, 0.5 mg ml^{-1}, or 1.0 mg ml^{-1} purified AmDH, 24 h or 48 h, 30°C. Error bars represent standard deviations of two independent experiments.

Increase of Butan-2-one and 1-Methoxypropan-2-one Concentration

Based on the screening results, we were prompted to test an increase in substrate concentration above 50 mM towards the small ketone butan-2-one (**1a**), which displayed a clear increase in yield between 10 and 50 mM. This study was conducted on *Msme*AmDH and the reaction was monitored at 24 h (**Figure 4A**). The already high ammonia concentration was retained at 2 M, the same ratio NH_4^+/substrate could not be maintained for reasons of solubility and ionic strenghts. The results obtained after UHPLC-UV analysis showed that 150 mM of **1a** was still converted in good yield (58.3%) to the corresponding (*S*)-amine **2a** with 0.5 mg ml^{-1} of *Msme*AmDH in 24 h. Even if the conversion dropped at 300 mM of substrate, the amount of amine formed was similar to that formed at 150 and 200 mM. The calculated *ee* values were similar for the amine **2a** whatever the initial substrate concentration, i.e., approximately, 91.8%–92.0%.

A similar study was performed for 1-methoxypropan-2-one (**1d**) at two different enzyme loadings (**Figure 4B**). The conversions were similar at 50–150 mM and decreased 1.4–1.7 times at 200 mM depending on the reaction duration and enzyme concentration. Running the reaction for 48 h with 0.5 mg ml^{-1} or 24 h with twice the amount of enzyme enabled 81.7%–85.9% conversion of 100 mM of ketone, which were roughly the conversions obtained at 50 mM (74.0–85.9%). At 200 mM, the conversions did not exceed 58% whatever the conditions used, which were still similar to that obtained at 10 mM during the screening in 96-well plates (56.5%). At 200 mM, the space time yields were 5.2–7.9 g L^{-1} day^{-1}, depending on the reaction time and enzyme loading.

Semi-preparative Synthesis of (*S*)-MOIPA ((*S*)-2d) and (*S*)-Butan-2-amine ((*S*)-2a)

In view of the tolerance to high loadings of 1-methoxypropan-2-one **1d** and butan-2-one **1a**, the semi-preparative syntheses of (*S*)-MOIPA ((*S*)-**2d**) and (*S*)-**2a** were performed to highlight the potential of these enzymes, and more particularly of wild-type *Msme*AmDH. Therefore, the synthesis of (*S*)-MOIPA was carried out at 7.5 mmol scale at 150 mM substrate concentration over 48 h with 0.5 mg ml^{-1} of *Msme*AmDH. Based on calibration

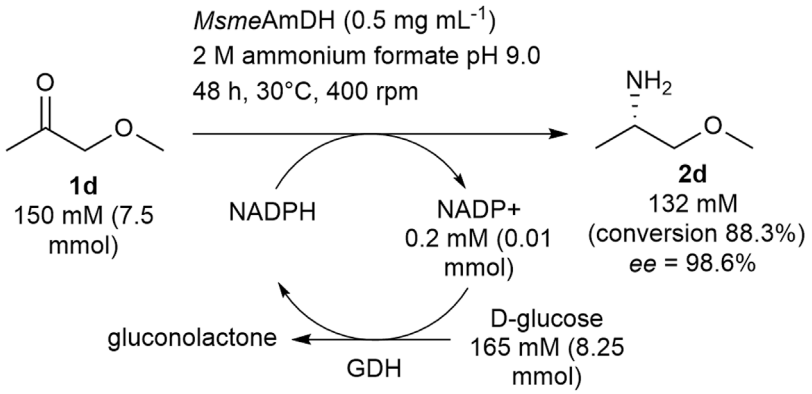

FIGURE 5 | Semi-preparative synthesis of (*S*)-1-methoxypropan-2-amine (*S*)-**2d**.

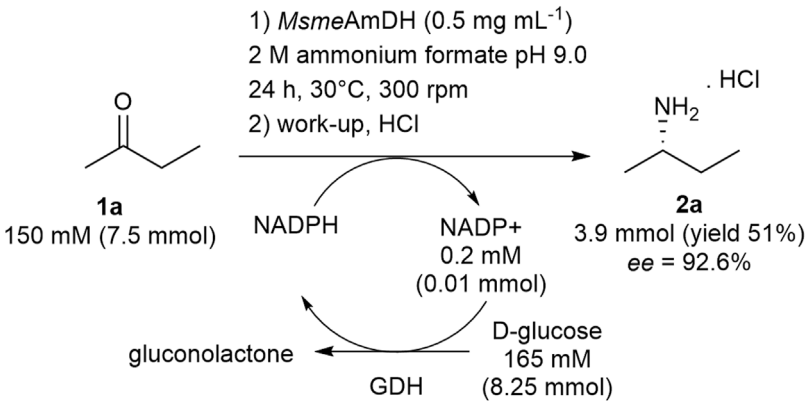

FIGURE 6 | Semi-preparative synthesis of (*S*)-butan-2-amine (**2a**).

curves, 6.6 mmol of (*S*)-MOIPA was formed (88.3% conversion, *ee* = 98.6%), superior to the result on the 100-µl scale, probably due to a better control of the reaction conditions at larger scale (**Figure 5**). Isolation of the product was not performed due to high water solubility and volatility of the product but the established industrial synthesis of this compound is evidence for the feasibility of this process step.

The synthesis of **2a** was also carried out at the 7.5 mmol scale at 150 mM substrate concentration over 24 h with 0.5 mg ml^{-1} of *Msme*AmDH. The resulting conversion (>99%) was again higher than the one obtained at the 100-µl scale. Following a similar protocol to the one described by Heckmann et al., the desired (*S*)-butan-2-amine (**2a**) was isolated thanks to a distillation procedure with 51% yield and 92.6% *ee* after added lyophilization step (**Figure 6**).

Modeling Studies

Taking advantage of the crystallographic structures of *Msme*AmDH and *Cfus*AmDH with their cofactor $NADP^+$ (PDB ID: 6IAQ and 6IAU, respectively), molecular docking using some tested amines and the closed form of *Msme*AmDH-$NADP^+$ or *Cfus*AmDH-NADP+ were performed using Autodock software (Morris et al., 2009). In addition, *Micro*AmDH was modeled by homology using the closed form of *Msme*AmDH (PDB ID: 6IAQ) as a template, as already described for MATOUAmDH2 with *Cfus*AmDH as a template (Caparco et al., 2020). Molecular docking was performed on these models following the same procedure as on *Msme*AmDH or *Cfus*AmDH. Among the fifty docking conformations obtained from the docking simulations (docking protocol detailed in Materials and Methods), the ratio between correct conformations harboring (*S*)-stereochemistry and those having (*R*)-stereochemistry was analyzed (**Figure 7**). As the final step of the reductive amination mechanism is the transfer of the hydride from C4 of the nicotinamide ring of the NAD(P)H cofactor to the C atom of the iminium intermediate to give respectively the oxidized $NAD(P)^+$ and the amine product, only conformations having the correct orientation of the hydrogen toward the cofactor were selected.

As detailed in **Figure 7**, for the butan-2-amine (**2a**) ligand, a majority of (*S*)-conformations were generated with the correct orientation in *Cfus*AmDH, *Msme*AmDH, and MATOUAmDH2,

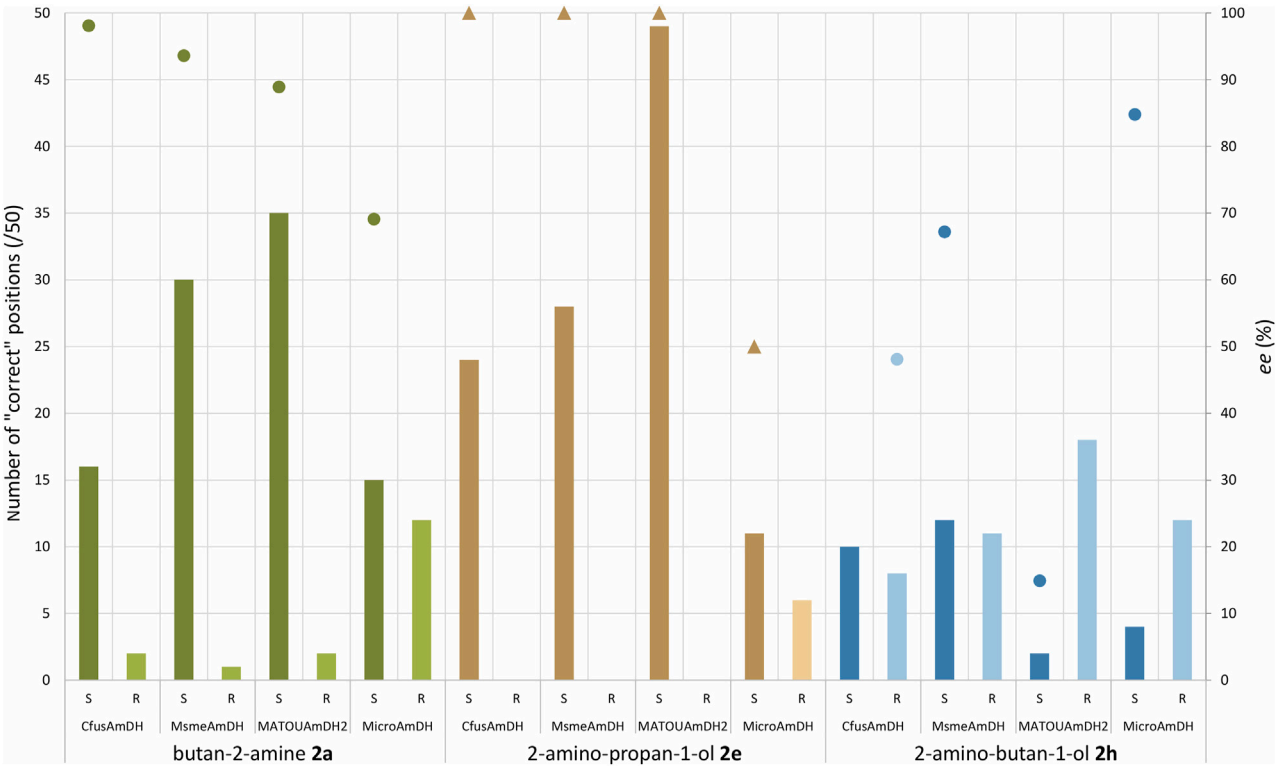

FIGURE 7 | Docking simulation of (*S*)- and (*R*)-amines 2a, 2e, and 2h. Bars represent the number of "correct" positions obtained out of 50 generated conformations while the scatter plot represents the enantiomeric excess obtained from the corresponding reaction (circles: calculated experimental data, triangles: estimated experimental data). *ee* values are indicated for (*S*)-amines except for **2h** with *Cfus*AmDH which is for (*R*)-**2h**. For **2e** ligand, *ee* values could not be determined but (*R*)-**2e** was only found in traces with *Cfus*AmDH, *Msme*AmDH, and MATOUAmDH2 (*ee* values arbitrarily indicated at 100%) but was obtained in larger proportion with *Micro*AmDH (*ee* arbitrarily indicated at 50%).

respectively 16, 30, and 35 out of 50 poses while the (*R*)-conformations gave respectively only 2, 1, and 2 correct positions out of 50 poses. On the other hand, for *Micro*AmDH, the difference is much lower with 15 out of 50 poses of (*S*)-conformations and 12 out of 50 poses of (*R*)-conformations. These *in silico* results are in accordance with the experimental data that showed good *ee* values for the first three enzymes (88.9%–98.1%) while *Micro*AmDH reached only a 69.1% *ee* with this substrate.

Based on the docking results, the different (*R*)/(*S*) ratios are difficult to explain as the positioning of the docked amines in their (*R*) and (*S*) conformations is almost identical, as illustrated in **Figure 8** in the case of *Msme*AmDH. No clear correlation between residues surrounding the substrate, or residues of the second layer, and the docking results with each enzyme could be established. Possibly, the features of the docking algorithm, such as the assumption of rigid protein and ligand, can obscure the reasons for these differences in enantioselectivity.

A good correlation between *in silico* and *in vitro* results was observed with the 2-amino-propan-1-ol (**2e**) ligand, for which only (*S*)-enantiomers were obtained both from these docking studies and from the biocatalytic reactions with *Cfus*AmDH, *Msme*AmDH, and MATOUAmDH2. Without being quantified, some (*R*)-**2e** was only experimentally identified with *Micro*AmDH while also being docked in 35% correct conformations [11/50 for (*S*)-conformation against 6/50 for (*R*)-conformation]. This different enantioselectivity and (*R*)-/(*S*)-ratios obtained with *Micro*AmDH with **2e** can be due to a coordination by hydrogen bonding of the hydroxyl group of the ligand with the hydroxyl group of Y169 (P11), which can favor the positioning of the ketone for the formation of the corresponding (*R*)-amine (**Figure 9**). If we use the nomenclature already published (Mayol et al., 2019), where the residues composing the active site pocket were renamed as their spatial positions P1 to P20, this key residue is P11. Both mechanistic and structural roles have been postulated for P3 as the catalytic residue while P11 was hypothesized to be essential for the closing of the active site (Mayol et al., 2019). As a reminder, alignment of these P1–P20 residues in the studied AmDHs is presented in **Figure 10**.

In *Cfus*AmDH and MATOUAmDH2, P11 is also occupied by Y, respectively Y173 and Y176, but with a slightly different position that moves the hydroxyl group further away from the ligand (Δ = 0.4 Å between Y169 of *Micro*AmDH and Y173 of *Cfus*AmDH, and Δ = 0.8 Å between Y169 of *Micro*AmDH and Y176 of MATOUAmDH2). In addition, the more hindered W164 (P9) in *Micro*AmDH compared to Y168 and Y171 in *Cfus*AmDH and MATOUAmDH2 can also impart less flexibility to the

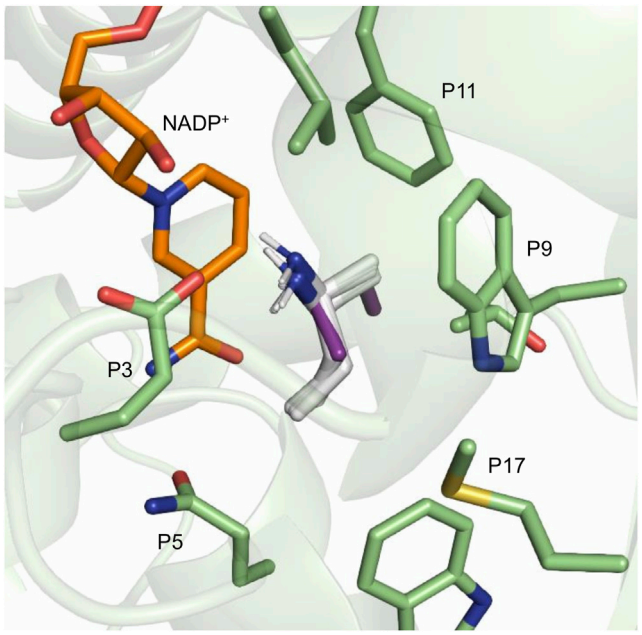

FIGURE 8 | *Msme*AmDH RX structure (PDB: 6IAQ) and NADP$^+$ cofactor, in orange, with docked structures of (*S*)-**2a**, in white, and (*R*)-**2a**, in purple. All the (*S*)-**2a** docked structures belong to the 20 conformations displaying the lowest binding energy.

alkylhydroxyl chain. In the docking poses, the latter is oriented more towards Y169 in *Micro*AmDH and its hydroxyl group, increasing access to (*R*)-configurations. In *Msme*AmDH, P11 is occupied by a phenylalanine that cannot provide a hydrogen bond with the substrate to favor the formation of the (*R*)-amine. In that case, only (*S*)-**2e** can be docked with the hydroxyl group orientated towards the carboxylate function of the glutamate in P3, with which a hydrogen bond can occur (**Figure 8**).

For 2-aminobutanol (**2h**) ligand, overall, the *in silico* analysis revealed much more (*R*)-poses with all the enzymes compared to the other ligands, which is in accordance with the *in vitro* analysis displaying the lowest *ee* values for this amine. For example, in *Msme*AmDH, approximately the same number of (*S*)- and (*R*)-correct poses were obtained, and the *ee* value for the (*S*)-**2h** was experimentally 67%. Nevertheless, the higher *ee*s obtained experimentally for *Micro*AmDH and *Msme*AmDH compared to MATOUAmDH2 and *Cfus*AmDH are not directly related to the respective ratios of correct (*R*)- and (*S*)-conformations in this modeling study. For example, in MATOUAmDH2, the ratio of (*R*)/(*S*) poses was higher than with *Cfus*AmDH, whereas *Cfus*AmDH facilitated the formation of (*R*)-**2h** with an *ee* value of 48% and MATOUAmDH2 facilitated the formation of (*S*)-**2h** with an *ee* value of 15%. For *Cfus*AmDH and *Msme*AmDH, this ratio was similar (respectively 8/10 and 11/12), whereas *Msme*AmDH displayed a clear preference for the formation of (*S*)-**2h** (*ee* = 67%). For *Cfus*AmDH, many (*R*)-poses seemed stabilized with the hydroxyl group of Y173 (**Figure 11A**), thus explaining the greatest rate of formation of (*R*)-amines compared to other substrates, even if the *ee* value remained low ($ee_{(R)}$ = 48.1%). The more hindered ethyl moiety of (*R*)-**2h**, compared to (*R*)-**2e**, might "push" the rotation of the substrate, still keeping the chiral center close to the NADP$^+$ hydride carbon, and make the hydroxyl group closer to the tyrosine even in *Cfus*AmDH (2 Å) and MATOUAmDH2 (2.9 Å). It is noticeable that for MATOUAmDH2 and *Msme*AmDH, the different conformations displayed much more variability of positions, explained structurally by the presence of other residues (P5, P8, P9, P16, and P17) surrounding these key positions, thus enabling other interactions and positioning of the key residues potentially less visible in these models (**Figure 11B**).

DISCUSSION

In addition to the protein engineering work that can be performed to access valuable biocatalysts, the deep characterization of wild-type enzymes selected from biodiversity is also a very efficient strategy. This study showed that recently described native AmDHs (*Cfus*AmDH, *Msme*AmDH, *Micro*AmDH, and MATOUAmDH2) appear as suitable biocatalysts for sustainable access to very small chiral amines. This was exemplified by moderate to high conversion rates obtained with 2-amino C3-C5 alkanes at high substrate loadings, and with hydroxylated 2-aminoalkanes such as (3*S*)-3-aminobutan-2-ol (**2g**)

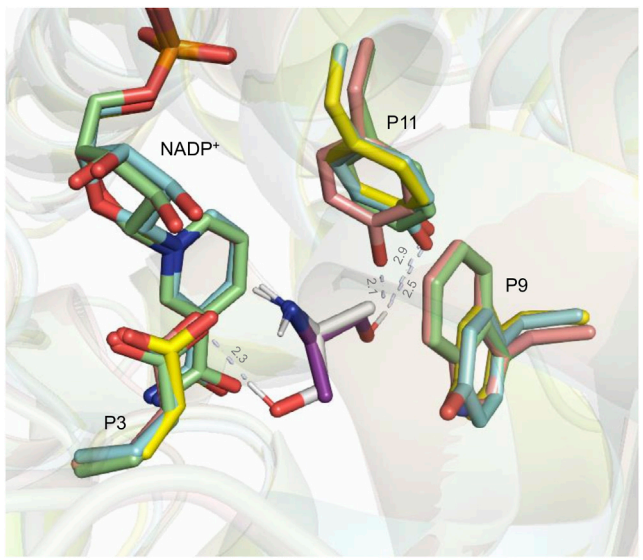

FIGURE 9 | Structural alignment of *Cfus*AmDH RX structure (PDB: 6IAU; blue), *Micro*AmDH homology model (PDB template: 6IAQ; pink), and MATOUAmDH2 homology model (PDB template: 6IAU; yellow) to *Msme*AmDH RX structure (PDB: 6IAQ; green). The corresponding NADP$^+$ cofactors are shown in the same color as the enzyme to which they belong. Docked structures of (*S*)-**2e** and (*R*)-**2e** in *Micro*AmDH are respectively shown in white and purple. The distance between the hydrogen atom of the hydroxyl group of (*S*)-**2e** and the oxygen atom of the carboxylate group of E104 (P3) in *Micro*AmDH, and between the hydrogen atom of the hydroxyl group of (*R*)-**2e** and the oxygen atom of the hydroxyl group of Y169, Y173, and Y176 (P11), respectively, of *Micro*AmDH, *Cfus*AmDH, and MATOUAmDH2, are given in Å.

	P1	P2	P3	P4	P5	P6	P7	P8	P9	P10	P11	P12	P13	P14	P15	P16	P17	P18	P19	P20
*Cfus*AmDH	S84	G107	E108	G139	Q141	F144	W145	T166	Y168	N169	Y173	L177	H181	P200	S201	Y202	C269	G271	T301	T305
*Msme*AmDH	S80	S103	E104	G135	Q137	F140	W141	A162	W164	N165	F169	L173	Q177	P197	T198	F199	M266	G268	T298	T302
*Micro*AmDH	S80	S103	E104	G135	Q137	F140	W141	S162	W164	N165	Y169	L173	Q177	P196	T197	F198	M265	G267	T297	T301
MATOUAmDH2	S87	A110	E111	G142	L144	A147	C148	L169	Y171	N172	Y176	L180	H184	K209	S210	Y211	Q278	G280	T312	T316

FIGURE 10 | Comparison of the active site residues P1–P20 of the selected AmDHs. All the P1 to P20 residues listed come from an alignment with *Cfus*AmDH (PDB: 6IAU). The color code used refers to the polarity and charge of the corresponding residue [blue: polar residues, yellow: hydrophobic residues, orange: aromatic residues, red: negatively charged residues, and green: positively charged residues (charges at physiological pH)].

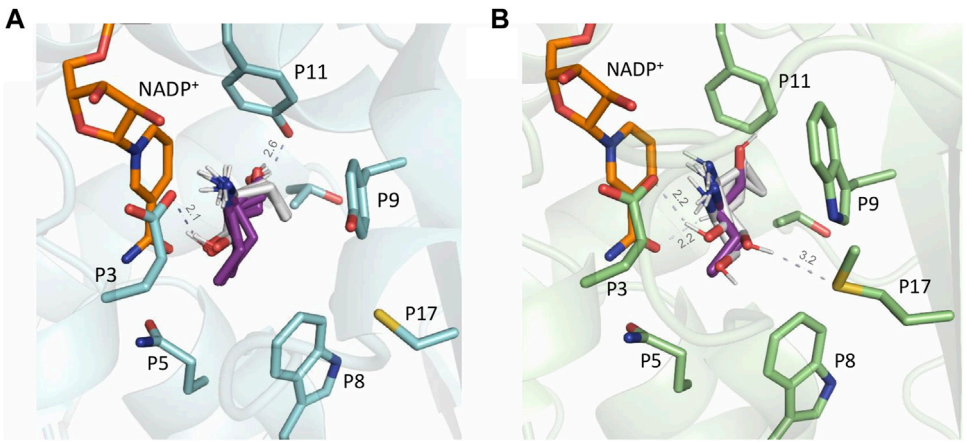

FIGURE 11 | (A) *Cfus*AmDH RX structure (PDB: 6IAU) and $NADP^+$ cofactor, in orange, with docked structures of (*S*)-**2e**, in white, and (*R*)-**2e**, in purple; **(B)** *Msme*AmDH RX structure (PDB: 6IAQ) and $NADP^+$ cofactor, in orange, with docked structures of (*S*)-**2e**, in white, and (*R*)-**2e**, in purple.

and (*S*)-1-methoxypropan-2-amine (**2d**), (*S*)-MOIPA. Despite its modeled larger catalytic pocket, MATOUAmDH2 displayed similar conversion rates and very high *ee* values, even if it seemed less well adapted for hydroxy ketones. The studied amines, challenging to obtain at high *ee* values due to inherent similarly sized substituents, are obtained with good to very good *ee* values with these enzymes. They are therefore positioned perfectly as a complement to the only few enzymes performing chemical reductive amination already described on these small ketones. Particularly, they differ from the imine reductase studied by Johnson-Matthey and Turner's group reported to be active toward 1-methoxypropan-2-one (**1d**) but with an alkylated amine and not ammonia as amine source, and without further published details (Montgomery et al., 2020). In view of their previously described substrate scope, these native AmDHs clearly displayed preference for small substrates, and particularly these 2-aminoketones with C3–C5 carbon chain length, whereas RedAms such as *Nf*RedAm, *At*RedAm, or *Ad*RedAm have been shown to be active toward carbon chain of C6 length or above and again mostly with larger amines than ammonia (Sharma et al., 2018; González-Martínez et al., 2020; Mangas-Sanchez et al., 2020). Compared to the engineered enzymes, only the modified AADH L-AmDH-TV was reported to be active toward the short C4 aliphatic ketones butan-2-one (**1b**). This modified leucine DH derived from *Bacillus stearothermophilus* displayed interesting specific activities toward pentan-2-one (**1c**) (1,303.6 mU mg^{-1}), and, in a lesser extent, toward butan-2-one (**1b**) (225.5 mU mg^{-1}) (Franklin et al., 2020). The absence of conversion data with these substrates does not allow to compare this enzyme more accurately with our native AmDHs. For the higher homolog **1c**, both L-AmDH-TV and the mutant LE-AmDH-v1 from the ε-deaminating L-lysine dehydrogenase from *Geobacillus stearothermophilus* appeared to be more efficient biocatalysts (Tseliou et al., 2019). Nevertheless, their opposite enantioselectivity renders them complementary enzymes to *Cfus*AmDH, *Msme*AmDH, and MATOUAmDH2, but not alternative ones. Regarding the hydroxyl-functionalized tested ketones, the studied native AmDHs seemed competitive compared to the mutant AmDH-M_0 displaying very interesting biocatalytic capabilities for the synthesis of different chiral vicinal amino alcohols. Even if no conversion data were reported by Chen et al. for the C3 amine **2e** and the C4 amine **2f**, the commonly studied amine (2*S*)-aminobutan-1-ol (**2h**) was obtained after a 24 h reaction with AmDH-M_0 with 91% conversion and *ee* > 99% at 30°C starting from 50 mM substrate concentration (Chen et al., 2019). Taking into account that the data provided here for hydroxylated ketones may be underestimated due to a study carried out in 96-well plates, and that the work of Chen et al. was performed with a triple amount of purified enzyme, similar conversions (70%–90%) may be reached with *Micro*AmDH for **2h**, a precursor of the drug ethambutol. Further improvement should permit higher tolerance to higher substrate concentrations and higher *ee* values for this substrate. Interestingly,

the authors suggested a favorable coordination of the hydroxyl group of the ligand with some key residues, as we postulated here with Y in P11 in some native AmDHs. In their case, the hydroxyl group of 1-hydroxypentan-2-one may interact with the mutated residue T68, the same as for the carboxylic moiety of the amino acid in the AADH native enzyme. To access amines (*S*)-**2e** and (*S*)-**2f** *via* reductive amination, especially with high enantioselectivity, *Msme*AmDH and *Cfus*AmDH seemed to be the only described dehydrogenases.

Concerning enzymes not performing reductive amination, many data have been reported with TAs. For example, the (*S*)-1-methoxypropan-2-one (**2d**) was synthesized with a ω-TA (Höhne and Bornscheuer, 2009). Despite the completely different mechanism of action between TAs and reductive aminases such as AmDHs, we discussed here some results obtained with TAs to underline the key role of AmDHs in the biocatalytic synthesis of such compounds. Native AmDHs and more particularly *Msme*AmDH seemed complementary to HewT or *RTA-X43 used by Heckmann et al. for the continuous-flow synthesis of butan-2-amine (**2a**). If we refer to the data provided in batch conditions without immobilization for more accurate comparison, *Msme*AmDH behaves similarly to HewT or *RTA-X43 in terms of conversion increase with higher substrate loadings in the range 10–100 mM, but not above. Both TAs displayed similar or higher conversions at 300 mM compared to 100 mM, whereas conversions with *Msme*AmDH drastically dropped above 150 mM. This behavior tends to suggest that these TAs have higher affinity for higher homologs than **1a** whereas *Msme*AmDH seemed more designed for small substrates such as **1a**–**1h**, but limited by very high substrate loadings. *Msme*AmDH favored the formation of the (*S*)-amine like HewT but with higher *ee* values (91% at 150 mM vs. 45% at 100 mM). Further exploration of AmDH homologs may enable the selection of (*R*)-selective AmDHs for **1a**, to provide an alternative to *RTA-X43, highly stereoselective for the (*R*)-amine formation. Again, protein engineering on *Msme*AmDH may also help to improve from the currently good *ee* value to excellent *ee* value for this target. As successfully demonstrated by the authors with TAs, scale-up synthesis of **2a** in flow with these AmDHs may provide alternative process systems, also potentially extendable to at least **2b**–**2d**, especially as these AmDHs do not require the use of a sacrificial amine donor such as isopropylamine (IPA), which clearly complicates the purification of the target amine. As exemplified in this work, the distillation protocol greatly elaborated by Paradisi et al. for **2a** has been facilitated here by the absence of IPA.

*Cfus*AmDH and *Msme*AmDH are also complementary to *Rb*TA, a (*R*)-selective TA applied by Li et al. for the synthesis of various (*R*)-hydroxyl amines such as (*R*)-ABOL (**2f**). *Cfus*AmDH and *Msme*AmDH harbor a less narrow substrate scope, as *Rb*TA can convert C4-C7 ketones, but furnish the opposite (*S*)-enantiomer, thus widening the biocatalytic solutions for accessing such chiral building blocks. Obtained here in non-optimal condition in a 96-well plate with 48%–66% yield with excellent (*S*)-stereoselectivity (*ee* > 99%), the opposite enantiomer (*S*)-**2f** ((*S*)-ABOL) could be synthesized with *Msme*AmDH or *Cfus*AmDH without requiring high loading of IPA as it was done by Li et al. with 1 M IPA for 100 mM substrate **1f** and 30 g L^{-1} of whole cells in 60 h (Li et al., 2021). Again, Y125 in *Rb*TA was postulated to play a key role in substrate hydroxy ketone recognition by forming a hydrogen bond with the hydroxyl functionality according to docking results and loss of activity with the mutation Y125A, thus supporting our hypothesis of key role of P11 in our case.

The structurally based preliminary explanation of the slight differences in (*S*)-enantioselectivities observed experimentally for **2a**–**2g**, together with the important variability for **2h**, helps to better understand the enzyme-substrate interactions within the catalytic pockets of these four enzymes. It would be interesting to perform some deeper computational studies, including molecular dynamics simulations, as done by Tseliou et al., to explain the substrate-dependent stereo-switchable selectivity in the case of the mutant LE-AmDH-v1 (Tseliou et al., 2019). *In silico* studies with the iminium intermediates or carbinolamines, instead of the amine products, may provide additional explanations for the different rates of enantioselectivity observed depending on AmDHs and substrates.

This study highlights the potential of native AmDHs, especially *Cfus*AmDH, *Msme*AmDH, *Micro*AmDH and MATOUAmDH2, for the biocatalytic synthesis of short aliphatic amines and hydroxy amines. For the latter, in one simple step, high conversion rates and *ee* values can be reached, which is remarkable compared to conventional synthesis. Due to high (*S*)-enantioselectivity, they are perfectly complementary to the few reductive amination enzymes described for these substrates, which are mostly (*R*)-selective. They are also positioned as very good alternatives to TAs such as *RTA-X43. (*S*)-MOIPA currently produced by the ChiPros™ process at more than 5,000 tons per year is a nice example of what can be achieved with these native enzymes (non-optimized STY 7.9 g L^{-1} day^{-1} with *Msme*AmDH). Protein engineering work coupled with the structural analysis provided should improve their efficiency and use in chemical synthesis.

DATA AVAILABILITY STATEMENT

The original contributions presented in the study are included in the article/**Supplementary Material**. Further inquiries can be directed to the corresponding author.

AUTHOR CONTRIBUTIONS

CV-V conceived the project. LD, CV-V designed and conducted the experiments, with input of AC and MB. LD, GG, and CV-V analyzed data with input from AZ, AB, and JC. LD and CV-V wrote the manuscript with input from GG, AZ, AC, and AB. All authors read and approved the final manuscript.

FUNDING

This study was supported by the Commissariat à l'Énergie Atomique et aux Énergies Alternatives (CEA), the CNRS and the University of Evry Val d'Essonne.

ACKNOWLEDGMENTS

The authors thank P. Wincker and V. de Berardinis for supporting the project, P. Sirvain and A. Perret for large-scale purification of the described enzymes, O. Maciejak (University Val d'Essonne) for NMR assistance, and the Region Ile de France for financial support of the 600-MHz spectrometer.

SUPPLEMENTARY MATERIAL

The Supplementary Material for this article can be found online at: https://www.frontiersin.org/articles/10.3389/fctls.2021.781284/full#supplementary-material

REFERENCES

Ager, D. J., Prakash, I., and Schaad, D. R. (1996). 1,2-Amino Alcohols and Their Heterocyclic Derivatives as Chiral Auxiliaries in Asymmetric Synthesis. *Chem. Rev.* 96, 835–876. doi:10.1021/cr9500038

Bradford, M. M. (1976). A Rapid and Sensitive Method for the Quantitation of Microgram Quantities of Protein Utilizing the Principle of Protein-Dye Binding. *Anal. Biochem.* 72, 248–254. doi:10.1016/0003-2697(76)90527-3

Caparco, A. A., Pelletier, E., Petit, J. L., Jouenne, A., Bommarius, B. R., Berardinis, V., et al. (2020). Metagenomic Mining for Amine Dehydrogenase Discovery. *Adv. Synth. Catal.* 362, 2427–2436. doi:10.1002/adsc.202000094

Chen, F.-F., Cosgrove, S. C., Birmingham, W. R., Mangas-Sanchez, J., Citoler, J., Thompson, M. P., et al. (2019). Enantioselective Synthesis of Chiral Vicinal Amino Alcohols Using Amine Dehydrogenases. *ACS Catal.* 9, 11813–11818. doi:10.1021/acscatal.9b03889

Cheng, F., Li, Q., Li, H., and Xue, Y. (2020). NAD(P)H-dependent Oxidoreductases for Synthesis of Chiral Amines by Asymmetric Reductive Amination of Ketones. *Sheng Wu Gong Cheng Xue Bao* 36, 1794–1816. doi:10.13345/j.cjb.190582

Cosgrove, S. C., Ramsden, J. I., Mangas-Sanchez, J., and Turner, N. J. (2021). "Biocatalytic Synthesis of Chiral Amines Using Oxidoreductases," in *Methodologies in Amine Synthesis: Challenges and Applications*. Editors A. Ricci and L. Bernardi (Weinheim: Wiley VCH), 243–283. doi:10.1002/9783527826186.ch7

Ditrich, K. (2020). "Optically Active Amines on an Industrial Scale," in *Amine Biocatalysis* (Stuttgart, Germany), 4.

Ducrot, L., Bennett, M., Grogan, G., and Vergne-Vaxelaire, C. (2020). NAD(P)H-Dependent Enzymes for Reductive Amination: Active Site Description and Carbonyl-Containing Compound Spectrum. *Adv. Synth. Catal.* 363, 328–351. doi:10.1002/adsc.202000870

Franklin, R. D., Mount, C. J., Bommarius, B. R., and Bommarius, A. S. (2020). Separate Sets of Mutations Enhance Activity and Substrate Scope of Amine Dehydrogenase. *ChemCatChem* 12, 2436–2439. doi:10.1002/cctc.201902364

Gomm, A., and O'Reilly, E. (2018). Transaminases for Chiral Amine Synthesis. *Curr. Opin. Chem. Biol.* 43, 106–112. doi:10.1016/j.cbpa.2017.12.007

González-Martínez, D., Cuetos, A., Sharma, M., García-Ramos, M., Lavandera, I., Gotor-Fernández, V., et al. (2020). Asymmetric Synthesis of Primary and Secondary β-Fluoro-arylamines Using Reductive Aminases from Fungi. *ChemCatChem* 12, 2421–2425. doi:10.1002/cctc.201901999

Heckmann, C. M., Dominguez, B., and Paradisi, F. (2021). Enantio-Complementary Continuous-Flow Synthesis of 2-Aminobutane Using Covalently Immobilized Transaminases. *ACS Sustain. Chem. Eng.* 9, 4122–4129. doi:10.1021/acssuschemeng.0c09075

Höhne, M., and Bornscheuer, U. T. (2009). Biocatalytic Routes to Optically Active Amines. *ChemCatChem* 1, 42–51. doi:10.1002/cctc.200900110

Koszelewski, D., Pressnitz, D., Clay, D., and Kroutil, W. (2009). Deracemization of Mexiletine Biocatalyzed by ω-Transaminases. *Org. Lett.* 11, 4810–4812. doi:10.1021/ol901834x

Li, F., Liang, Y., Wei, Y., Zheng, Y., Du, Y., and Yu, H. (2021). Biochemical and Structural Characterization of an (R)-Selective Transaminase in the Asymmetric Synthesis of Chiral Hydroxy Amines. *Adv. Synth. Catal.* 363, 4582–4589. doi:10.1002/adsc.202100636

Mangas-Sanchez, J., Sharma, M., Cosgrove, S. C., Ramsden, J. I., Marshall, J. R., Thorpe, T. W., et al. (2020). Asymmetric Synthesis of Primary Amines Catalyzed by Thermotolerant Fungal Reductive Aminases. *Chem. Sci.* 11, 5052–5057. doi:10.1039/d0sc02253e

Mayol, O., Bastard, K., Beloti, L., Frese, A., Turkenburg, J. P., Petit, J.-L., et al. (2019). A Family of Native Amine Dehydrogenases for the Asymmetric Reductive Amination of Ketones. *Nat. Catal.* 2, 324–333. doi:10.1038/s41929-019-0249-z

Montgomery, S. L., Pushpanath, A., Heath, R. S., Marshall, J. R., Klemstein, U., Galman, J. L., et al. (2020). Characterization of Imine Reductases in Reductive Amination for the Exploration of Structure-Activity Relationships. *Sci. Adv.* 6, eaay9320. doi:10.1126/sciadv.aay9320

Morris, G. M., Huey, R., Lindstrom, W., Sanner, M. F., Belew, R. K., Goodsell, D. S., et al. (2009). AutoDock4 and AutoDockTools4: Automated Docking with Selective Receptor Flexibility. *J. Comput. Chem.* 30, 2785–2791. doi:10.1002/jcc.21256

Mutti, F. G., and Knaus, T. (2021). "Enzymes Applied to the Synthesis of Amines," in *Biocatalysis for Practitioners: Techniques, Reactions and Applications*. Editors D. G. Gonzalo and I. Lavandera (Weinheim: Wiley VCH), 143–180. doi:10.1002/9783527824465.ch6

Patil, M. D., Grogan, G., Bommarius, A., and Yun, H. (2018a). Oxidoreductase-Catalyzed Synthesis of Chiral Amines. *ACS Catal.* 8, 10985–11015. doi:10.1021/acscatal.8b02924

Patil, M. D., Grogan, G., Bommarius, A., and Yun, H. (2018b). Recent Advances in ω-Transaminase-Mediated Biocatalysis for the Enantioselective Synthesis of Chiral Amines. *Catalysts* 8, 254. doi:10.3390/catal8070254

Rehn, G., Ayres, B., Adlercreutz, P., and Grey, C. (2016). An Improved Process for Biocatalytic Asymmetric Amine Synthesis by *In Situ* Product Removal Using a Supported Liquid Membrane. *J. Mol. Catal. B: Enzymatic* 123, 1–7. doi:10.1016/j.molcatb.2015.10.010

Sharma, M., Mangas-Sanchez, J., France, S. P., Aleku, G. A., Montgomery, S. L., Ramsden, J. I., et al. (2018). A Mechanism for Reductive Amination Catalyzed by Fungal Reductive Aminases. *ACS Catal.* 8, 11534–11541. doi:10.1021/acscatal.8b03491

Slabu, I., Galman, J. L., Lloyd, R. C., and Turner, N. J. (2017). Discovery, Engineering, and Synthetic Application of Transaminase Biocatalysts. *ACS Catal.* 7, 8263–8284. doi:10.1021/acscatal.7b02686

Tseliou, V., Knaus, T., Masman, M. F., Corrado, M. L., and Mutti, F. G. (2019). Generation of Amine Dehydrogenases with Increased Catalytic Performance and Substrate Scope from ε-deaminating L-Lysine Dehydrogenase. *Nat. Commun.* 10, 3717. doi:10.1038/s41467-019-11509-x

Wu, S., Snajdrova, R., Moore, J. C., Baldenius, K., and Bornscheuer, U. T. (2021). Biocatalysis: Enzymatic Synthesis for Industrial Applications. *Angew. Chem. Int. Ed.* 60, 88–119. doi:10.1002/anie.202006648

Ye, L. J., Toh, H. H., Yang, Y., Adams, J. P., Snajdrova, R., and Li, Z. (2015). Engineering of Amine Dehydrogenase for Asymmetric Reductive Amination of

Ketone by Evolving *Rhodococcus* Phenylalanine Dehydrogenase. *ACS Catal.* 5, 1119–1122. doi:10.1021/cs501906r

Conflict of Interest: The authors declare that the research was conducted in the absence of any commercial or financial relationships that could be construed as a potential conflict of interest.

Publisher's Note: All claims expressed in this article are solely those of the authors and do not necessarily represent those of their affiliated organizations, or those of the publisher, the editors, and the reviewers. Any product that may be evaluated in this article, or claim that may be made by its manufacturer, is not guaranteed or endorsed by the publisher.